Jurnal Teknologi

Full Paper

MODIFICATION OF THE ANAND CONSTITUTIVE MODEL FOR ENHANCING PREDICTIVE ACCURACY OF 96.5SN-3.0AG-0.5CU INELASTIC DEFORMATION BEHAVIOR

Aliff Farhan Mohd Yamin[a,b], Jamaluddin Mahmud[a]*

[a]Faculty of Mechanical Engineering, Universiti Teknologi MARA, 40450 Shah Alam, Selangor, Malaysia
[b]Faculty of Mechanical Engineering, Universiti Teknologi MARA Cawangan Pulau Pinang, Permatang Pauh Campus, 13500 Seberang Prai, Pulau Pinang, Malaysia

Article history
Received
2 August 2024
Received in revised form
31 December 2024
Accepted
31 December 2024
Published Online
22 August 2025

*Corresponding author
jm@uitm.edu.my

Graphical abstract

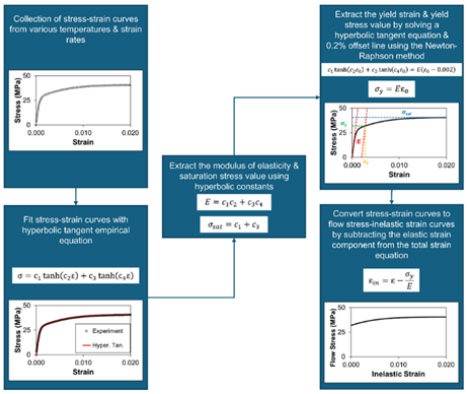

Abstract

This paper presents the modification and improvement of the Anand constitutive model for accurately predicting the mechanical behavior of 96.5Sn-3.0Ag-0.5Cu (SAC305) lead-free solder. The original Anand model had limitations in capturing strain hardening significantly at low-strain applications. The modified Anand model addressed this limitation by correlating the initial value of deformation resistance (s_0) and hardening coefficient (h_0) as a temperature and strain rate function. The Anand and modified Anand model parameters were determined through two-stage optimization-type curve fitting using Genetic Algorithm (GA) and Nelder-Mead (NM) optimization methods. Experimental data indicated good agreement with both models. However, the modified Anand model showed a significantly lower MSE (0.2216) than the Anand model (0.3396), suggesting improved agreement with experimental data. The modified model's yield and saturation stress prediction were also enhanced, with maximum errors of 4.36% and 4.39%, respectively. The modified Anand model also exhibited higher coefficient of determination (R^2) value (0.9996), surpassing the original model's R^2 value of 0.9981. These results demonstrated the enhanced predictive capability of the modified model at various conditions. Thus, the modified Anand model could represent the SAC305 solder joint deformation behavior.

Keywords: Anand Model, creep, SAC305, solder joint, stress-strain

Abstrak

Kertas kerja ini membentangkan pengubahsuaian dan penambahbaikan model konstitutif Anand untuk meramalkan dengan tepat tingkah laku mekanikal sambungan pateri bebas plumbum 96.5Sn-3.0Ag-0.5Cu (SAC305). Model Anand amat terhad dalam meramal pengerasan terikan pada aplikasi terikan rendah. Model Anand yang diubah suai menangani isu ini dengan mengubah suai nilai awal rintangan ubah bentuk (s_0) dan pekali pengerasan (h_0) sebagai fungsi suhu dan kadar terikan. Parameter Anand dan Anand yang diubah suai ditentukan melalui pencocokan lengkung jenis pengoptimuman dua peringkat menggunakan Algoritma Genetik (GA) dan Nelder-Mead (NM). Hasil pencocokan lengkung menunjukkan hubungan baik antara kedua-dua model dengan data eksperimen. Walau bagaimanapun, ralat kuasa dua minimum (MSE) Anand yang diubah suai menunjukkan MSE yang jauh lebih rendah (0.2216) berbanding model Anand (0.3396). Ramalan tegasan alah dan tegasan tepu juga ditambah baik untuk model yang

diubah suai menghasilkan ralat maksimum masing-masing sebanyak 4.36% dan 4.39%. Ini menunjukkan model Anand yang diubah suai lebih mendekati dapatan eksperimen berbanding model Anand. Model Anand yang diubah suai juga menunjukkan nilai pekali penentuan (R^2) yang lebih tinggi (0.9996), mengatasi nilai R^2 model Anand iaitu 0.9981. Keputusan ini menunjukkan keupayaan ramalan model Anand yang diubah suai yang dipertingkatkan merentasi pelbagai keadaan. Oleh itu, pengubahsuaian yang dilakukan pada model Anand menunjukkan penambahbaikan ramalan tingkah laku SAC305 berbanding model Anand.

Kata kunci: Model Anand, rayapan, *SAC305,* sambungan pateri, tegasan-terikan

1.0 INTRODUCTION

In electronic packaging, solder joints are crucial in interconnecting electronic components on printed circuit boards (PCBs), providing mechanical support and electrical conduction. As electronic products continue to advance in functionality and miniaturization, the decreasing size of solder joints poses reliability challenges [1, 2]. Therefore, it becomes crucial to understand the mechanical behavior of solder joints under various operating conditions to ensure their reliability.

During thermal cyclic loading, solder joints experience inelastic deformation due to mismatches in thermal expansion between different adjacent materials [3]. The accumulation of inelastic strain over time is a crucial factor in determining the reliability of these solder connections. Typically, the inelastic strain range remains below 10% under such thermal loading conditions [4]. Accurately predicting this inelastic strain behavior is essential to capturing the complex deformation mechanisms within solder joints, thereby improving our understanding of their performance and durability.

The Anand model has been widely employed to numerically describe the inelastic behavior of solder alloys. Initially developed for lead solder alloys, this model has also been extended to lead-free solder, such as 96.5Sn-3.0-Ag-0.5Cu (SAC305). The Anand model offers a unified approach to describe the mechanical behavior of solder alloys and effectively captures the influence of temperature and strain rate on solder joint deformation [5, 6]. It can be efficiently implemented in finite element (FE) models, enabling accurate stress and strain distribution calculation in solder joints under different loading conditions [7–11]. Extensive validation has demonstrated the Anand model's accuracy in predicting the solder's stress-strain relationship under uniaxial monotonic loading.

Previous studies have utilized the Anand model to investigate various aspects of solder joint behavior. Zhang *et al*. (2014) examined the deformation behavior of solder joints during board-level drop tests and found that the Anand model accurately predicted the inelastic strain at high strain rates [6]. Motalab *et al*. (2016) employed the Anand model to simulate the creep behavior of lead-free solder joints in microelectronic packages, successfully captured the time-dependent deformation and provided accurate predictions of long-term reliability [12]. Talledo *et al*. (2021) developed a new power equation for the Quad Flat No-Lead (QFN) packages for fatigue prediction models based on accumulated creep strain energy density from Finite Element Analysis (FEA) simulations [13]. The study highlighted the Anand model's ability to accurately predict the solder joint lifetime in the QFN packages.

Despite its widespread use, the Anand model has certain limitations. It inaccurately predicts the inelastic behavior of solder material at low-strain applications, often overpredicting the flow stress in such regions [14]. Additionally, the model must accurately predict solder joint behavior under complex loading conditions, especially in cyclic loading [14]. Unreliable models can result in overpredicted inelastic strain, which, in turn, may lead to premature detection of fracture or failure in electronic packages.

To address these limitations, researchers have proposed modifications to the Anand model. Parameter refinement is a popular approach, improving the model's accuracy in predicting solder joint behavior under various loading conditions, including complex loading applications. This approach involves adjusting the model parameters to better capture solder joints' behavior.

Several studies have focused on modifying the parameters in the Anand model to enhance its predictive capability. Rizaman *et al*. (2024) proposed an improved Anand model specifically for 96.5Sn-4.0-Ag-0.5Cu (SAC405) lead-free solder used in microelectronic packages [15]. The modification focused on the three parameters of the Anand model (s_0, h_0 and $\hat{s}$). By introducing temperature and strain rate dependence for these parameters, more accurate predictions of the inelastic deformation behavior of the SAC405 solder were achieved. Similarly, Xu Long *et al*. (2020) refined two Anand model parameters (s_0 and a) to improve the prediction of plastic ball grid array (PBGA) packages under thermal cyclic loading [16]. Sn37-Pb63 and SAC305 solders data from the tensile test were used to calibrate their model. It was demonstrated that the

parameterized Anand model could effectively predict the deformation and failure mechanisms of solder materials across a wide range of temperatures and strain rates.

This study applied the Anand constitutive model by modifying two critical parameters, namely the initial value of deformation resistance (s_0) and hardening coefficient (h_0). Parameters of the modified Anand model were acquired from SAC305 uniaxial tensile experiments encompassing temperatures ranging from 25°C to 125°C and strain rates ranging from 10^{-5} s^{-1} to 10^{-3} s^{-1}[17]. The model capability was assessed by comparing the flow stress predicted by the modified model with the original Anand model and SAC305 experimental data. The modified Anand model is anticipated to improve the predictive capability compared to the unmodified Anand model.

2.0 METHODOLOGY

2.1 Mathematical Development of the Anand and Modified Anand Models

The total strain (ε) in the solder material can be decomposed into elastic strain (ε_e) and inelastic strain (ε_{in}) components as defined in Equation (1).

$$\varepsilon = \varepsilon_e + \varepsilon_{in} \tag{1}$$

The elastic strain follows Hooke's law. In the classical strain model, the inelastic strain is expressed as a linear combination of time-independent plastic strain (ε_p) and time-dependent creep strain (ε_{crp}), as given in Equation (2).

$$\varepsilon_{in} = \varepsilon_{pl} + \varepsilon_{crp} \tag{2}$$

Equation (2) has a significant limitation as it tends to overestimate the total strain, particularly under cyclic loading conditions. This overestimation leads to inaccuracy in the computed hysteresis curves, which worsens the fatigue life estimation of solder joints [18]. Additionally, separating creep and plastic deformation in experimental measurements poses a challenge, further necessitating the development of a unified model to predict solder deformation accurately [19].

The unified inelastic strain model addresses these issues by consolidating all inelastic deformation components, including plastic strain (ε_{pl}) and creep strain (ε_{crp}), into a single inelastic strain term. This integration improves the model's predictive accuracy, offering a more robust framework for solder joint applications. As a result, the unified approach has gained widespread acceptance to numerically simulate the deformation behavior of solder joints. Among various unified constitutive models, the Anand model is the most widely adopted to capture the complex deformation behavior of solder alloys [7–11].

The Anand model was initially developed to describe the hot-working mechanical behavior of metals under high-temperature conditions [20, 21]. The model used an internal scalar variable (s) to represent the isotropic resistance to inelastic flow offered by the internal state of the material. It unifies the solder's creep and rate-independent plastic behavior by utilizing stress, flow, and evolution equation. For uniaxial loading, the flow stress is computed using Equation (3).

$$\sigma = cs \tag{3}$$

where, s is the internal variable, and c is the strain rate and temperature function, as expressed in Equation (4).

$$c = \frac{1}{\xi}\sinh^{-1}\left[\left(\frac{\dot{\varepsilon}_{in}}{A}\mathrm{e}^{\frac{Q}{RT}}\right)^{m}\right] \tag{4}$$

where, $\dot{\varepsilon}_{in}$ is the inelastic strain rate, T is the absolute temperature, ξ is stress multiplier, A is the pre-exponential factor, Q is the activation energy, R is the universal gas constant, and m is the strain rate sensitivity. Substituting and rearranging Equations (3) and (4) results in the flow equation of the Anand model expressed in Equation (5).

$$\dot{\varepsilon}_{in} = A\mathrm{e}^{-\frac{Q}{RT}}\left[\sinh\left(\xi\frac{\sigma}{s}\right)\right]^{\frac{1}{m}} \tag{5}$$

The value of deformation resistance constantly changes over time and can be expressed numerically by Equation (6).

$$\dot{s} = \left[h_0\left|1-\frac{s}{s^*}\right|^{a}\operatorname{sign}\left(1-\frac{s}{s^*}\right)\right] \tag{6}$$

where, h_0 is the hardening constant, a is the strain rate sensitivity of the hardening process and s^* is the saturation stress at a given temperature and strain rate. The value of s^* in Equation (6) can be computed using Equation (7).

$$s^* = \hat{s}\left(\frac{\dot{\varepsilon}_{in}}{A}\mathrm{e}^{\frac{Q}{RT}}\right)^{n} \tag{7}$$

where, $\hat{s}$ is the deformation resistance coefficient, and n is the strain rate sensitivity of the saturation value of the deformation resistance. For $s < s^*$, Equation (6) can be rewritten in incremental form as indicated in Equation (8).

$$\mathrm{d}s = h_0\left(1-\frac{s}{s^*}\right)^{a}\mathrm{d}\varepsilon_{in} \tag{8}$$

The s value is determined by integrating Equation (8) with inelastic strain (ε_{in}).

$$s = s^* - \left[(s^*-s_0)^{(1-a)} + (a-1)h_0\varepsilon_{in}(s^*)^{-a}\right]^{\frac{1}{1-a}} \tag{9}$$

where, s_0 is the initial value of s. Substituting Equation (7) into Equation (9) yields the expanded version of internal state variable s, as expressed by Equation (10).

$$s = \hat{s}\left(\frac{\dot{\varepsilon}_{in}}{A}e^{\frac{Q}{RT}}\right)^n - \left\{\begin{array}{c}\left[\hat{s}\left(\frac{\dot{\varepsilon}_{in}}{A}e^{\frac{Q}{RT}}\right)^n - s_0\right]^{(1-a)} + \\ h_0(a-1)\varepsilon_{in}\left[\hat{s}\left(\frac{\dot{\varepsilon}_{in}}{A}e^{\frac{Q}{RT}}\right)^n\right]^{-a}\end{array}\right\}^{\frac{1}{1-a}} \quad (10)$$

By substituting Equations (4) and (10) into Equation (3), the flow stress as a function of inelastic strain, temperature, and strain rate can be described by Equation (11).

$$\sigma = \left\{\begin{array}{c}\left(\frac{1}{\xi}\sinh^{-1}\left[\left(\frac{\dot{\varepsilon}_{in}}{A}e^{\frac{Q}{RT}}\right)^m\right]\right) \\ \left(\hat{s}\left(\frac{\dot{\varepsilon}_{in}}{A}e^{\frac{Q}{RT}}\right)^n - \left\{\begin{array}{c}\left[\hat{s}\left(\frac{\dot{\varepsilon}_{in}}{A}e^{\frac{Q}{RT}}\right)^n - s_0\right]^{(1-a)} + \\ h_0(a-1)\varepsilon_{in}\left[\hat{s}\left(\frac{\dot{\varepsilon}_{in}}{A}e^{\frac{Q}{RT}}\right)^n\right]^{-a}\end{array}\right\}^{\frac{1}{1-a}}\right)\end{array}\right\} \quad (11)$$

For accurate prediction, especially at low-strain applications, two Anand model parameters were selected, namely s_0 and h_0. These two parameters are defined as a function of temperature and strain rate, as depicted in Equations (12) and (13) from previous studies [16, 22].

$$s_0 = c_0 + c_1T + c_2T^2 \quad (12)$$

$$h_0 = k_0 + k_1T + k_2T^2 + k_3\dot{\varepsilon}_{in} + k_4{\dot{\varepsilon}_{in}}^2 \quad (13)$$

The s_0 and h_0 parameters control the overall shape of the flow stress-inelastic strain relation in the Anand model. The s_0 parameter defines the yield strength of the corresponding flow stress-inelastic strain curve (intersection at the y-axis). The h_0 parameter governs the slope of the flow stress-inelastic strain. The effects of changing s_0 and h_0 can be summarized in Figure 1.

By substituting Equations (12) and (13) into Equation (11), the predicted flow stress for the modified Anand model is expressed by Equation (14).

$$\sigma = \left\{\begin{array}{c}\frac{1}{\xi}\sinh^{-1}\left[\left(\frac{\dot{\varepsilon}_{in}}{A}e^{\frac{Q}{RT}}\right)^m\right] \\ \left(\hat{s}\left(\frac{\dot{\varepsilon}_{in}}{A}e^{\frac{Q}{RT}}\right)^n - \left\{\begin{array}{c}\left[\hat{s}\left(\frac{\dot{\varepsilon}_{in}}{A}e^{\frac{Q}{RT}}\right)^n - \right]^{(1-a)} + \\ (c_0 + c_1T + c_2T^2) \\ (k_0 + k_1T + k_2T^2 + k_3\dot{\varepsilon}_{in} + k_4{\dot{\varepsilon}_{in}}^2) \\ (a-1)\varepsilon_{in}\left[\hat{s}\left(\frac{\dot{\varepsilon}_{in}}{A}e^{\frac{Q}{RT}}\right)^n\right]^{-a}\end{array}\right\}^{\frac{1}{1-a}}\right)\end{array}\right\} \quad (14)$$

For the Anand model, only nine parameters (A, ξ, Q/R, m, h_0, a, s_0, $\hat{s}$, and n) were determined. However, for the modified model, a total of 15 parameters were needed (A, ξ, Q/R, m, a, $\hat{s}$, n, c_0, c_1, c_2, k_0, k_1, k_2, k_3, and k_4) to predict the inelastic behavior of the solder alloys. These parameters of the Anand and modified Anand models were determined through optimization-type curve fitting techniques.

2.2 Preparation of Flow Stress-Inelastic Strain Experimental Data

The stress-strain curves obtained from different temperatures and strain rates were essential for determining the Anand and modified Anand model parameters. In previous study, Motalab *et al*. (2013) extracted the SAC305 stress-strain curves at various temperatures (25°C, 50°C, 75°C, 100°C and 125°C) and strain rates (10^{-5} s^{-1}, 10^{-4} s^{-1}, and 10^{-3} s^{-1}) [17]. These stress-strain curves were converted into flow stress-inelastic strain curves using the 0.2% strain offset method.

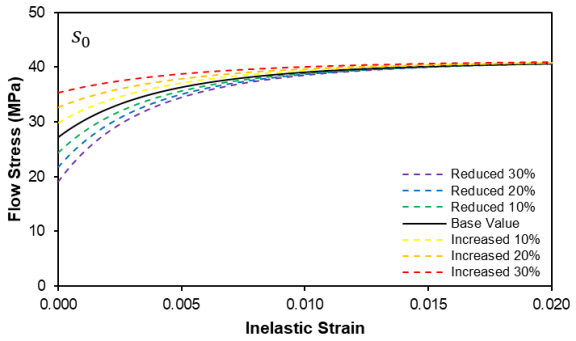

(a)

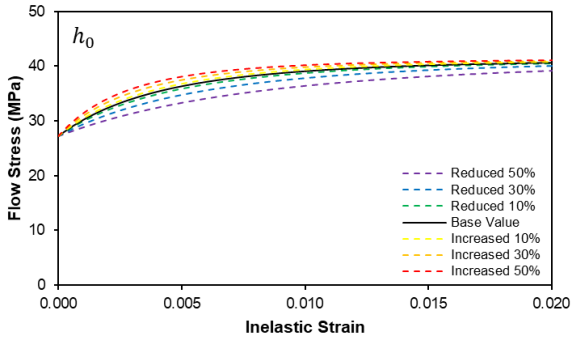

(b)

Figure 1 Effects of changing Anand model parameters: a) s_0 and b) h_0 [23]

The conversion process involved determining the modulus of elasticity (E), yield strength (σ_y), and saturation stress (σ_{sat}). The modulus of elasticity was determined by examining the linear elastic region of the stress-strain curve, where the material can return to its original length after unloading. The E values at various temperatures and strain rates are calculated using Equation (15), which is the change of stress ($\Delta\sigma$) to the change in strain ($\Delta\varepsilon$).

$$E = \frac{\Delta\sigma}{\Delta\varepsilon} \quad (15)$$

SAC305 solder alloy, like many materials, does not exhibit a distinct yield point where the stress-strain curve suddenly transitions from elastic to inelastic deformation. Instead, the curve transitions gradually,

making determining an exact yield point difficult. ASTM E8/E8M-24 standard proposed 0.2% to 2.0% strain offset in determining the yield strength of the metals [24]. This study chose the 0.2% strain offset to minimize the nonlinearity at the elastic region near the yield point. An offset of 0.2% strain with a slope equal to E determined the yield point. The offset line can be represented mathematically by Equation (16). The intersection of this line with the stress-strain curve indicates the yield strength of the material.

$$\sigma = E(\varepsilon - 0.002) \tag{16}$$

The stress-strain behavior of the solder alloy can be effectively modeled using the hyperbolic tangent empirical model, as introduced by Suhling (1985) [25], expressed in Equation (17).

$$\sigma = c_1 \tanh(c_2\varepsilon) + c_3 \tanh(c_4\varepsilon) \tag{17}$$

Suhling and his colleagues utilized the hyperbolic tangent model to fit the stress-strain relation of solder alloy obtained from experiment testing [17, 26]. The good predictive capability of the hyperbolic tangent empirical model with the experimental data indicates the model's reliability in predicting the solder alloys' stress-strain relation.

The extracted stress-strain curves from published literature at different temperatures and strain rates were fitted to Equation (17). The hyperbolic tangent empirical model could substitute the graphical 0.2% offset line technique in finding the modulus of elasticity, yield strength, and ultimate tensile strength (saturation stress). Using Equation (17), the saturation stress (σ_{sat}) of the solder alloy can be determined using Equation (18) by assuming a nearly constant stress value at a prolonged strain condition ($\varepsilon \to \infty$).

$$\sigma_{sat} = \lim_{\varepsilon \to \infty} \sigma = \sigma(\infty) = c_1 + c_3 \tag{18}$$

The instantaneous slope of the stress-strain curve, which can be used to find the modulus of elasticity (E), is determined by differentiating Equation (17) and yield Equation (19).

$$\frac{d\sigma}{d\varepsilon} = c_1 c_2 \operatorname{sech}^2(c_2\varepsilon) + c_3 c_4 \operatorname{sech}^2(c_4\varepsilon) \tag{19}$$

The value of E can be found in Equation (20) by assuming the slope value at zero strain condition ($\varepsilon \to 0$).

$$E = \lim_{\varepsilon \to 0} \frac{d\sigma}{d\varepsilon} = c_1 c_2 + c_3 c_4 \tag{20}$$

Equation (20) can be used to describe the modulus of elasticity (E) for each stress-strain curve. The value strain at the yield point (ε_y) can be determined by combining Equations (16) and (17), thus generating Equation (21).

$$c_1 \tanh(c_2\varepsilon_y) + c_3 \tanh(c_4\varepsilon_y) = E(\varepsilon_y - 0.002) \tag{21}$$

Since Equation (21) is a non-linear expression (cannot be solved directly), the indirect procedure must be utilized to find the ε_y value. By utilizing the Newton-Raphson method in Equation (21), the value of ε_y can be found. Subsequently, the yield strength (σ_y) can be computed using Equation (22).

$$\sigma_y = E\varepsilon_y \tag{22}$$

The inelastic strain (ε_{in}) is calculated as the difference between the total strain (ε) and the elastic strain (ε_e) obtained from the linear portion of the stress-strain curve as described in Equation (23).

$$\varepsilon_{in} = \varepsilon - \frac{\sigma_y}{E} \tag{23}$$

Each extracted stress-strain curve is converted into its corresponding flow stress-inelastic strain by identifying the modulus of elasticity, yield stress, and saturation stress. After identifying these properties, by using Equation (23), the flow stress-inelastic strain can be determined.

Figure 2 shows the process flow of converting stress-strain from the extracted experimental data to flow stress-inelastic strain of SAC305 solder alloy at various temperatures and strain rates.

2.3 Extraction of the Model Parameters

Recent advancements in computational speed and optimization algorithms have revolutionized parameter identification. Pei and Qu (2005) applied neural networks (NN) to effectively determine Anand model parameters for 96.6Sn-3.5Ag and 95.5Sn-3.8Ag-0.7Cu solder alloys [27]. Subsequently, Qinghua Su *et al*. (2023) demonstrated the utility of NN in determining Anand model parameters for SAC305 [28]. The NN approach eliminates the multi-step procedures to determine model parameters as introduced by previous researchers [20, 21]. Additionally, Zhao Zhang (2019) utilized an evolving type of algorithm to identify Anand model parameters for SAC305, highlighting the versatility of contemporary optimization techniques [29]. Similarly, Martin Fusek *et al*. (2021) incorporated a modified genetic algorithm (GA) combined with sensitivity analysis and hill-climbing algorithms to determine Anand model parameters for ABS-M30 plastic utilized in 3D printing applications [30].

Evolving algorithms, including GA, enhance exploration and randomness in the optimization process, significantly facilitating the discovery of optimal solutions and mitigating the risk of entrapment in local optima [29]. In contrast to gradient methods that may converge to local minima, GA leverages a population-based approach, allowing the simultaneous exploration of multiple solutions. This characteristic is crucial when dealing with Anand

model parameters, as the parameter space can be highly non-linear and complex.

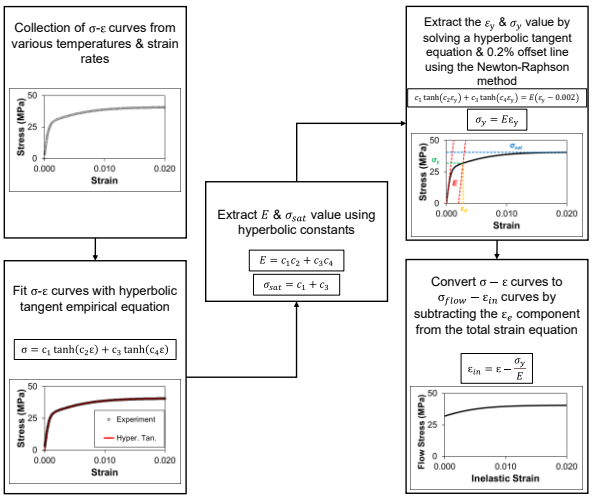

Figure 2 Flowchart of converting stress-strain curves of the extracted experimental data to flow stress-inelastic strain curves of SAC305 solder alloy

In this study, two-stage optimization technique was employed to find the optimal set of parameters of the Anand model (A, ξ, Q/R, m, h_0, a, s_0, $\hat{s}$, and n) and modified Anand model (A, ξ, Q/R, m, a, $\hat{s}$, n, c_0, c_1, c_2, k_0, k_1, k_2, k_3, and k_4). The first stage utilized GA as a meta-heuristic optimization method to explore the parameter space and identify the initial set of model parameters for the second stage of the optimization process (Nelder-Mead algorithm). The second stage optimization method was needed as a local search optimization technique to fine-tune the initial solution obtained from the GA optimization.

Figure 3 summarizes the process of determining Anand and modified Anand model parameters using two-stage optimization-type curve fitting. Initially, the process began with compiling the flow stress-inelastic strain dataset, essential for calibrating both models. Random values were then assigned to the model parameters to form the initial population for the GA.

The GA evolves this population over multiple generations through selection, crossover, and mutation operations. At each generation, the mean squared error (MSE) between the experimental flow stress (σ_{exp}) and predicted flow stress (σ_{pred}) is calculated to assess each parameter set, which is summarized in Equation (24).

$$MSE=\frac{1}{n}\sum\left(\sigma_{exp}-\sigma_{pred}\right)^2 \quad (24)$$

Solutions with lower MSE were selected for further crossover and mutation to improve performance. This iterative process continued until the GA converged, either by reaching a predefined number of generations or when no significant improvement in MSE was observed.

The best-performing parameter set from the GA was further refined using the Nelder-Mead (NM) simplex method for local optimization. The NM algorithm began by generating a simplex in the parameter space, which was then iteratively updated through reflection, expansion, contraction, and shrinkage steps. These steps evaluated the MSE of the newly generated points relative to the simplex and adjusted the parameter values accordingly to minimize the MSE. The algorithm continued iterating until the MSE converged below a specified threshold or after a maximum number of iterations.

The predicted flow stress in the Anand and modified Anand model is computed using Equations (11) and (14), respectively. After the two-stage optimization process, the model's parameter values were evaluated by comparing the predicted stress values with the experimental data. The fit quality was assessed based on MSE and coefficient of determination (R^2). The R^2 values quantify the goodness of fit between the predicted model and experimental data, as described in Equations (25) and (26).

$$R^2=1-\frac{\sum\left(\sigma_{exp}-\sigma_{pred}\right)^2}{\sum\left(\sigma_{exp}-\sigma_{avg}\right)^2} \quad (25)$$

$$\sigma_{avg}=\frac{1}{n}\sum\sigma_{exp} \quad (26)$$

where, σ_{avg} is the mean flow stress of the experimental data, and n is the total number of data points.

Table 1 Anand and modified Anand model parameters for SAC305

Parameter		Anand	Modified Anand
$\frac{Q}{R}$ (K^{-1})		11690	11396
A (s)		788	268
ξ		9.532	11.252
m		0.1578	0.0412
$\hat{s}$ (MPa)		43.59	77.81
n		0.0239	0.0477
a		0.9636	1.4529
s_0 (MPa)	c_0 (MPa)		219.5
	c_1 (MPa.K^{-1})	56.98	0.02151
	c_3 (MPa.K^{-2})		-5.8795×10^{-4}
h_0 (MPa)	k_0 (MPa)		38320
	k_1 (MPa.K^{-1})		-2240
	k_3 (MPa.K^{-2})	23148	9.4077
	k_4 (MPa.s)		-1.100×10^{8}
	k_5 (MPa.s^2)		5.792×10^{8}

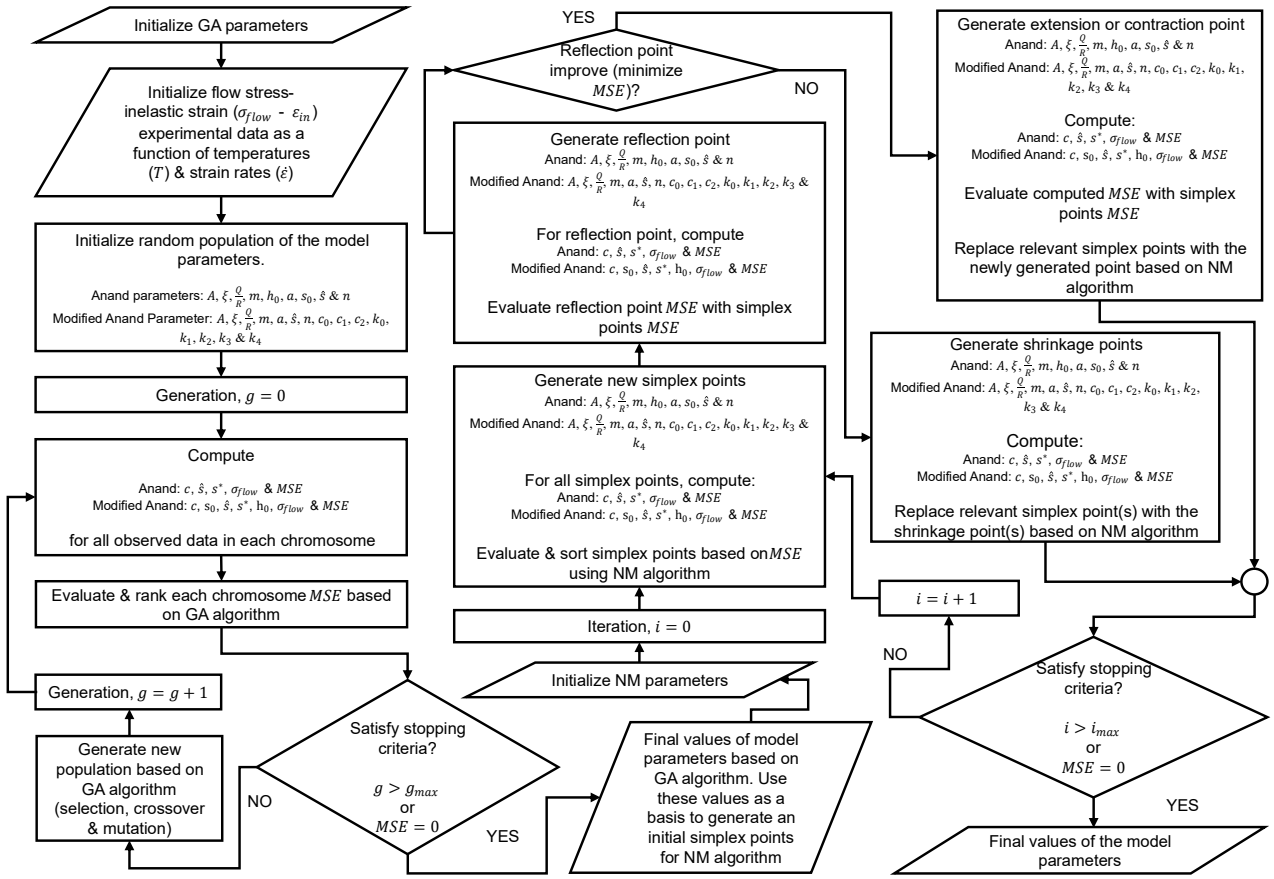

Figure 3 Flowchart of Anand and modified Anand model parameters determination using two-stage optimization type curve fittings for SAC305 solder alloy

Table 2 Comparison of predicted and experimental yield stress and saturation stress between Anand and modified Anand models

Temp. (°C)	Strain Rate (s^{-1})	Yield Stress					Saturation Stress				
		Exp.	Anand		Mod. Anand		Exp.	Anand		Mod. Anand	
		Value (MPa)	Value (MPa)	Error (%)	Value (MPa)	Error (%)	Value (MPa)	Value (MPa)	Error (%)	Value (MPa)	Error (%)
25	10^{-5}	24.25	24.77	2.14	24.00	1.03	29.26	30.39	3.86	30.28	3.49
	10^{-4}	26.66	26.13	1.99	26.18	1.80	35.55	35.01	1.52	35.57	0.06
	10^{-3}	27.17	28.35	4.34	27.50	1.21	40.52	40.06	1.14	40.85	0.81
50	10^{-5}	21.72	21.14	2.67	21.91	0.87	24.43	24.89	1.88	24.55	0.49
	10^{-4}	22.94	23.31	1.61	23.18	1.05	29.55	28.96	2.00	29.00	1.86
	10^{-3}	23.99	25.48	6.21	24.46	1.96	33.90	33.50	1.18	33.95	0.15
75	10^{-5}	17.91	19.38	8.21	18.69	4.36	20.13	20.68	2.73	20.41	1.39
	10^{-4}	20.76	20.55	1.01	20.86	0.48	24.66	24.15	2.07	24.39	1.09
	10^{-3}	21.47	23.03	7.27	21.75	1.30	27.90	28.45	1.97	28.48	2.08
100	10^{-5}	16.34	17.10	4.65	16.58	1.47	17.13	17.38	1.46	17.35	1.28
	10^{-4}	19.02	18.18	4.42	18.74	1.47	21.33	20.58	3.52	20.76	2.67
	10^{-3}	20.33	19.28	5.16	20.91	2.85	24.02	24.47	1.87	24.35	1.37
125	10^{-5}	14.99	14.74	1.67	15.02	0.20	15.45	14.74	4.60	15.02	2.78
	10^{-4}	15.53	16.90	8.82	16.00	3.03	17.08	17.85	4.51	17.83	4.39
	10^{-3}	18.57	17.00	8.45	19.06	2.64	21.42	21.17	1.17	21.28	0.65

3.0 RESULTS AND DISCUSSION

3.1 Anand and Modified Anand Model Parameters

This section compares the results of parameter determination of the Anand and modified Anand models obtained from the two-stage optimization-type curve fitting with the experimental data.

Table 1 shows the optimized parameter values of SAC305 solder material for Anand and modified Anand models. These parameters were crucial to accurately predict the SAC305 deformation behavior. The s_0 and h_0 values of the Anand model were constantly maintained for all temperatures and strain rate conditions. However, the s_0 and h_0 values of the modified Anand model depended on the temperatures and strain rates.

The modified Anand model introduced lower differences in A, ξ, Q/R, m, a, $\hat{s}$, and n values compared to the original Anand model. For instance, the Q/R value in the Anand model was reduced from 11690 K^{-1} to 11396 K^{-1} in the modified Anand model, indicating a change in the temperature sensitivity of the material. The ξ value also increased from 9.532 in the Anand model to 11.252 in the modified Anand model, suggesting an adjustment in the material's strain-hardening behavior. These modifications are expected to enhance the predictive capability of the modified Anand model.

The performance of the fit was evaluated by computing the overall MSE against the experimental data. The modified Anand model exhibited lower MSE of 0.2216 compared to that of the Anand model (0.3396). This value signified that the modified Anand model was more accurate in describing the transient relationship between flow stress and inelastic strain of SAC305 solder material. These additional parameters allowed for a more refined description of the material's response, leading to more accurate predictions.

3.2 Yield Stress and Saturation Stress Prediction of Anand and Modified Anand Models

A comparative analysis of the Anand and modified Anand models' predictive capabilities for yield and saturation stress is presented in Table 2. The predicted yield stress values ranged from 15 MPa to 27 MPa across strain rates of 10^{-5} s^{-1} to 10^{-3} s^{-1} and temperatures between 25°C and 125°C. The saturation stress values ranged from 15 MPa to 40 MPa under similar strain rates and temperatures. Both models followed the general trend of experimental data, with yield and saturation stresses decreasing as temperature increased, and both properties also reduced as the strain rate decreased.

When examining the prediction accuracy, the error margin for the yield stress of the Anand model ranged from 1.01% to 8.82%. In contrast, the modified Anand model achieved significantly reduced errors, ranging from 0.20% to 4.36%, indicating a clear improvement in accuracy. For the saturation stress prediction, the Anand model's errors ranged from 1.14% to 4.60%, whereas the modified Anand model further improved the accuracy with errors between 0.06% and 4.39%. The consistently lower error margins of the modified Anand model demonstrated its superior performance in predicting yield and saturation stresses at different environmental conditions. This enhanced capability highlighted the robustness of the modified model over the original Anand model.

At each specific condition, the modified Anand model showed improved predictive accuracy. For instance, at 25°C and strain rate of 10^{-5} s^{-1}, the modified model produced an error of only 1.03% compared to the original Anand model (2.14%). This trend was consistent in other conditions. At 50°C and strain rate of 10^{-3} s^{-1}, the modified model's error was 1.96%, significantly lower than the original model's error of 6.21%. These improvements were attributed to the modified model's capability to adjust the s_0 and h_0 values based on temperature and strain rate.

The Anand model demonstrated optimal accuracy for yield stress prediction at strain rate of 10^{-4} s^{-1} and temperature of 75°C. However, the least accurate prediction occurred at the same strain rate but at elevated temperature of 125°C. In contrast, the modified Anand model exhibited the best performance at strain rate of 10^{-5} s^{-1} and temperature of 125°C, although it performed less accurately at 10^{-5} s^{-1} strain rate and 75°C (environmental conditions).

Similarly, for the saturation stress prediction, the Anand model achieved the highest accuracy at strain rate of 10^{-3} s^{-1} and temperature of 25°C, and least accuracy at 10^{-5} s^{-1} strain rate and 125°C temperature. The modified Anand model, however, exhibited the most accurate prediction of the saturation stress at strain rate of 10^{-4} s^{-1} and temperature of 25°C, while its worst performance was seen at 10^{-4} s^{-1} strain rate and 125°C temperature.

Based on the comparative analysis of both models, the modified model demonstrated the superior predictive capability of yield and saturation stresses under different strain rates and temperatures. The modified Anand model consistently achieved lower error margins, offering more accurate and reliable predictions under various conditions.

3.3 Flow Stress-Inelastic Strain Prediction of Anand and Modified Anand Models

Figure 4 compares the flow stress-inelastic strain response predicted from the Anand and modified Anand models with experimental data at various temperatures (25°C to 125°C) and strain rates (10^{-5} s^{-1} to 10^{-3} s^{-1}). Both models showed reasonable agreement with the experimental data. Nevertheless, the modified Anand model demonstrated a more significant improvement in predicting the flow stress. This was evidenced by the specimen being tested at 10^{-3} s^{-1} and 25°C (Refer to Figure 4 (c)). The solid line

representing the flow stress predicted by the modified model was more closely aligned with the experimental data than the dotted line representing the unmodified model. From this situation, both models could also accurately predict the yield and saturation stresses in line with experimental observations. However, the evolution of the flow stress was quite different for both models. The predicted flow stress between yield and saturation stress was slightly overpredicted by the Anand model as opposed to the modified model due to the differences in the h_0 and a values. For this test condition, the a values of the Anand and modified Anand models were 0.9636 and 1.4529, respectively. Similarly, the h_0 values of the Anand and modified Anand models were 23 148 MPa and 96 719 MPa, respectively. These two parameters controlled the predicted values of the flow stress responses. As a result, the flow stress of the Anand model in this condition was more prone to early saturation than that of the modified model.

Table 3 Comparison of Anand and modified Anand models' R^2 values at different temperatures (25°C to 125°C) and strain rates (10^{-5} s^{-1} to 10^{-3} s^{-1}) for SAC305

Temp. (°C)	Strain Rate (s^{-1})	R^2	
		Anand	Mod. Anand
25	10^{-5}	0.1068	0.4579
	10^{-4}	0.9875	0.9983
	10^{-3}	0.9927	0.9996
50	10^{-5}	0.1022	0.9255
	10^{-4}	0.9785	0.9833
	10^{-3}	0.9981	0.9994
75	10^{-5}	-0.9013	0.5656
	10^{-4}	0.9848	0.9946
	10^{-3}	0.9933	0.9961
100	10^{-5}	-6.0384	-3.7527
	10^{-4}	0.9617	0.9756
	10^{-3}	0.9958	0.9983
125	10^{-5}	-165.1766	-59.7077
	10^{-4}	0.7715	0.7736
	10^{-3}	0.9971	0.9988

To quantitatively evaluate the predictive performance of the models, the R^2 value at each temperature and strain rate condition was calculated and is presented in Table 3. The R^2 values measured the proportion of variance in the experimental data captured by the models, with values approaching 1 indicating a good fit and near 0 indicating a poor fit. In Table 3, the modified Anand model outperformed the Anand model based on the R^2 values. For example, at 50°C and strain rate of 10^{-5} s^{-1}, the R^2 value of the modified Anand model was 0.9255, whereas the Anand model achieved R^2 value of 0.1022.

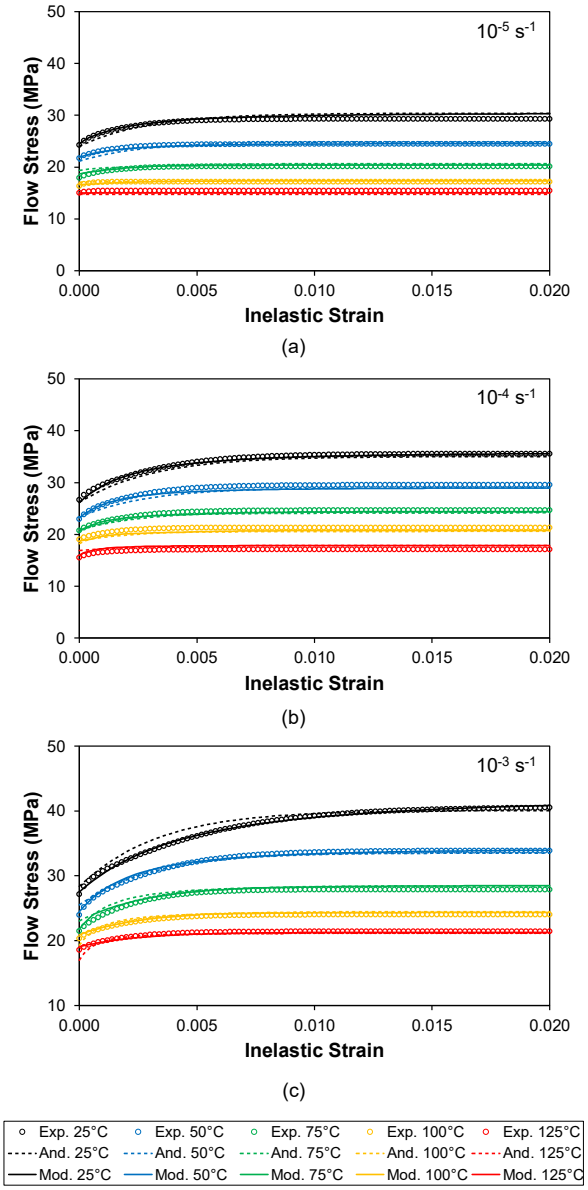

Figure 4 Predicted flow stress-inelastic strain responses of the Anand and modified Anand models at various temperatures (25°C - 125°C) and strain rates: a) 10^{-5} s^{-1}, b) 10^{-4} s^{-1}, and c) 10^{-3} s^{-1}

The maximum and minimum R^2 values of the Anand model were 0.9981 (10^{-3} s^{-1} and 50°C) and -165.1766 (10^{-5} s^{-1} and 125°C), respectively. For the modified Anand model, the maximum and minimum R^2 values were 0.9996 (10^{-3} s^{-1} and 25°C) and -59.7077 (10^{-5} s^{-1} and 125°C). It should be noted that the minimum R^2 values of both models were below zero. The negative R^2 values suggested that the models failed to capture the variation and trends exhibited by the experimental data under these conditions. Both models were less accurate for predicting flow stress at low strain rates (10^{-5} s^{-1}) and high temperatures.

However, the modified Anand model showed higher minimum R^2 value than the Anand model, indicating a lower risk in predicting the flow stress at lower strain and high temperature conditions. These results suggested that the capability of the modified Anand model to capture the material's response under varying conditions improved.

Overall, the accuracy of the modified Anand model significantly improved compared to the unmodified model. Modifying the model parameters of s_0 and h_0 resulted in reduced MSE and improved R^2 values. The increasing trend of R^2 values demonstrated improved predictive performance of the modified model under various conditions. The negative R^2 values highlighted the necessity of modifying the existing Anand model to accurately capture the material's response.

4.0 CONCLUSION

In conclusion, this study presents the modified Anand constitutive model to accurately predict the mechanical behavior of SAC305, a lead-free solder alloy. The modified Anand model demonstrated superior performance compared to the Anand model, as evidenced by the MSE values. The MSE value of the Anand model was 0.3396, whereas the modified Anand model achieved MSE value of 0.2216. This indicated a significantly reduced deviation from the experimental data.

The predictive capability of both models was evaluated by their accuracy in predicting yield and saturation stresses at various temperatures and strain rates. The modified Anand model yielded higher stress prediction error of 4.36% compared to 8.82% for the Anand model. For the saturation stress, the modified Anand model demonstrated a maximum error of 4.39%, while the Anand model yielded an error of 4.60%. The reduction in error affirmed the superior accuracy and robustness of the modified Anand model in capturing material behavior under varying conditions.

The predictive performance was also assessed by comparing the R^2 values of the flow stress-inelastic strain curves at different temperatures and strain rate conditions. The Anand model exhibited R^2 values ranging from a maximum of 0.9981 to a minimum of -165.1766. In contrast, the modified Anand model achieved R^2 values ranging from 0.9996 (maximum) and -59.7077 (minimum). Although both models produced negative R^2 values under certain conditions, the modified model significantly improved overall R^2 values and reduced the occurrence of negative R^2 values.

The results of this study suggested that the modified Anand model provided a more reliable framework for capturing the deformation behavior of SAC305 solder material. Its reduced error in predicting flow stress values makes it useful for future research to explore the model's applicability for other lead-free solder materials or alloys with similar creep and stress-relaxation behaviors.

Refining model parameters through experimental calibration at more extreme strain rates or temperature ranges may enhance its versatility across different applications, such as high-reliability electronic components.

Acknowledgement

This research was fully supported by the FRGS grant (FRGS/1/2021/TK0/UiTM/03/11). The authors fully acknowledge the Ministry of Higher Education (MOHE) and Universiti Teknologi MARA for the approved funds that made this study viable and effective.

Conflicts of Interest

The authors declare that there is no conflict of interest regarding the publication of this paper.

References

[1] Jiang, N., Zhang, L., Liu, Z.-Q., Sun, L., Long, W.-M., He, P., Xiong, M.-Y. and Zhao, M. 2019. Reliability Issues of Lead-free Solder Joints in Electronic Devices. *Science and Technology of Advanced Materials*. 20(1): 876–901. Doi: https://doi.org/10.1080/14686996.2019.1640072.

[2] Cheng, S., Huang, C.-M. and Pecht, M. 2017. A Review of Lead-free Solders for Electronics Applications. *Microelectronics Reliability*. 75: 77–95. Doi: https://doi.org/10.1016/j.microrel.2017.06.016.

[3] Li, L., Du, X., Chen, J. and Wu, Y. 2024. Thermal Fatigue Failure of Micro-Solder Joints in Electronic Packaging Devices: A Review. *Materials*. 17(10): 2365. Doi: https://doi.org/10.3390/ma17102365.

[4] Wei, X., Alahmer, A., Ali, H., Tahat, S., Vyas, P. P. and Hamasha, S. 2023. Effect of Temperature on the Low Cycle Fatigue Properties of BGA Solder Joints. *Microelectronics Reliability*. 146: 115031. Doi: https://doi.org/10.1016/j.microrel.2023.115031.

[5] Lall, P., Zhang, D., Yadav, V. and Locker, D. 2016. High Strain Rate Constitutive Behavior of SAC105 and SAC305 Leadfree Solder during Operation at High Temperature. *Microelectronics Reliability*. 62: 4–17. Doi: https://doi.org/10.1016/j.microrel.2016.03.014.

[6] Zhang, L., Han, J., Guo, Y. and He, C. 2014. Anand Model and FEM Analysis of SnAgCuZn Lead-free Solder Joints in Wafer Level Chip Scale Packaging Devices. *Microelectronics Reliability*. 54(1): 281–286. Doi: https://doi.org/10.1016/j.microrel.2013.07.100.

[7] Gharaibeh, M. A. 2023. Nonlinear Finite Element Simulations on the Mechanical Response of the Isothermally Aged Lead-Free Solders. *Proceedings of the Institution of Mechanical Engineers, Part L: Journal of Materials: Design and Applications*. 237: 11. Doi: https://doi.org/10.1177/14644207231179564.

[8] Depiver, J. A., Mallik, S. and Amalu, E. H. 2021. Thermal Fatigue Life of Ball Grid Array (BGA) Solder Joints Made from Different Alloy Compositions. *Engineering Failure Analysis*. 125: 105447. Doi: https://doi.org/10.1016/j.engfailanal.2021.105447.

[9] Depiver, J., Mallik, S. and Amalu, D. E. 2020. Comparing and Benchmarking Fatigue Behaviours of Various SAC Solders

under Thermo-Mechanical Loading. (Oct. 2020). Doi: https://doi.org/10.1109/ESTC48849.2020.9229699.
[10] Yamin, A. F. M., Abdullah, A. S., Manap, M. F. A. and Yusoff, H. 2019. Failure Prediction of the Solder Joints in the Ball-grid-array Package Under Thermal Loading. *Journal of Physics: Conference Series*. 1349(1): 012013. Doi: https://doi.org/10.1088/1742-6596/1349/1/012013.
[11] Yamin, A. F. M., Shaffiar, N. M., Loh, W. K. and Tamin, M. N. 2011. Damage Progression in BGA Solder Joints during Board-level Drop Test. *2011 IEEE 13th Electronics Packaging Technology Conference* (Dec. 2011). 681–685. Doi: https://doi.org/10.1109/EPTC.2011.6184504.
[12] Motalab, M., Mustafa, M., Suhling, J.C. and Lall, P. 2016. Improved Predictions of Cyclic Stress-strain Curves for Lead Free Solders using the Anand Viscoplastic Constitutive Model. *2016 15th IEEE Intersociety Conference on Thermal and Thermomechanical Phenomena in Electronic Systems (ITherm)* (May 2016). 471–480. Doi: https://doi.org/10.1109/ITHERM.2016.7517586.
[13] Talledo, J. 2021. Improving the Solder Joint Reliability Prediction Accuracy for Quad Flat No Lead Packages. *Journal of Engineering Research and Reports*. Doi: https://doi.org/10.9734/jerr/2021/v20i717344.
[14] Chen, G., Zhao, X. and Wu, H. 2017. A Critical Review of Constitutive Models for Solders in Electronic Packaging. *Advances in Mechanical Engineering*. 9(8): 1687814017714976. Doi: https://doi.org/10.1177/1687814017714976.
[15] Rizaman, M. S. A., Abdullah, A. S. and Yamin, A. F. M. 2024. Determination of the Anand Parameters for SAC405 Solders Through the Use of Stress-Strain Data. *Journal of Advanced Research in Applied Mechanics*. 113(1): 162–175. Doi: https://doi.org/10.37934/aram.113.1.162175.
[16] Long, X., Chen, Z., Wang, W., Fu, Y. and Wu, Y. 2020. Parameterized Anand Constitutive Model under a Wide Range of Temperature and Strain Rate: Experimental and Theoretical Studies. *Journal of Materials Science*. 55(24): 10811–10823. Doi: https://doi.org/10.1007/s10853-020-04689-1.
[17] Motalab, M., Mustafa, M., Suhling, J. C., Zhang, J., Evans, J., Bozack, M. J. and Lall, P. 2013. Correlation of Reliability Models Including Aging Effects with Thermal Cycling Reliability Data. *2013 IEEE 63rd Electronic Components and Technology Conference* (May 2013). 986–1004. Doi: https://doi.org/10.1109/ECTC.2013.6575694.
[18] Lee, W. W., Nguyen, L. T. and Selvaduray, G. S. 2000. Solder Joint Fatigue Models: Review and Applicability to Chip Scale Packages. *Microelectronics Reliability*. 40(2): 231–244. Doi: https://doi.org/10.1016/S0026-2714(99)00061-X.
[19] Che, F. X. and Pang, J. H. L. 2013. Fatigue Reliability Analysis of Sn–Ag–Cu Solder Joints Subject to Thermal Cycling. *IEEE Transactions on Device and Materials Reliability*. 13(1): 36–49. Doi: https://doi.org/10.1109/TDMR.2012.2195007.
[20] Anand, L. 1985. Constitutive Equations for Hot-working of Metals. *International Journal of Plasticity*. 1(3): 213–231. Doi: https://doi.org/10.1016/0749-6419(85)90004-X.
[21] Brown, S. B., Kim, K. H. and Anand, L. 1989. An Internal Variable Constitutive Model for Hot Working of Metals. *International Journal of Plasticity*. 5(2): 95–130. Doi: https://doi.org/10.1016/0749-6419(89)90025-9.
[22] Bo, L. Z., Kamsah, N., Keat, L. W. and Tamin, M. N. 2008. Mechanics of Sn-4Ag-0.5Cu Solder Joints in a Ball Grid Array Assembly during Reflow and Temperature Cycles. *2008 33rd IEEE/CPMT International Electronics Manufacturing Technology Conference (IEMT)* (Nov. 2008). 1–8. Doi: https://doi.org/10.1109/IEMT.2008.5507864.
[23] Motalab, M. 2013. *A Constitutive Model for Lead Free Solder Including Aging Effects and Its Application to Microelectronic Packaging*.
[24] ASTM E8/E8M-24 - Standard Test Methods for Tension Testing of Metallic Materials.
[25] Suhling, J. C. 1985. *Constitutive Relations and Failure Predictions for Nonlinear Orthotropic Media*. The University of Wisconsin - Madison.
[26] Hassan, K. R., Alam, M. S., Wu, J., Suhling, J. C. and Lall, P. 2020. Isothermal Aging Dependent Anand Parameters of SAC305 Lead Free Solder at Extreme High Temperatures. *2020 19th IEEE Intersociety Conference on Thermal and Thermomechanical Phenomena in Electronic Systems (ITherm)* (Jul. 2020). 1191–1200. Doi: https://doi.org/10.1109/ITherm45881.2020.9190596.
[27] Pei, M. and Qu, J. 2005. Constitutive Modeling of Lead-free Solders. *Proceedings. International Symposium on Advanced Packaging Materials: Processes, Properties and Interfaces, 2005.* (Mar. 2005). 45–49. Doi: https://doi.org/10.1109/ISAPM.2005.1432043.
[28] Su, Q., Yuan, C. and Chiang, K. N. 2023. Fitting Solder305 Anand Model Parameters with Artificial Neural Networks. *2023 18th International Microsystems, Packaging, Assembly and Circuits Technology Conference (IMPACT)* (Oct. 2023). 143–147. Doi: https://doi.org/10.1109/IMPACT59481.2023.10348916.
[29] Zhang, Z., Chen, Z., Liu, S. and Dong, F. 2019. Parameter Identification of Anand Constitutive Models for SAC305 using the Intelligent Optimization Algorithm. *2019 IEEE 21st Electronics Packaging Technology Conference (EPTC)* (Dec. 2019). 133–137. Doi: https://doi.org/10.1109/EPTC47984.2019.9026663.
[30] Fusek, M., Paška, Z., Rojíček, J. and Fojtík, F. 2021. Parameters Identification of the Anand Material Model for 3D Printed Structures. *Materials*. 14(3): 587. Doi: https://doi.org/10.3390/ma14030587.